Article

Scalable Resin Embedding Method for Large-Volume Brain Tissues with High Fluorescence Preservation Capacity

Tissue preparation

Dehydration/Penetration · Polymerization+4%AMS · Polymerization mechanism

Ferret brain · Macaque brain · Fluorescence signal

Data acquisition

Sectioning · Imaging

Knife

Specimen

Solution
PI+0.05M Na2CO3
+0.05M EDTA

Ting Luo, Lei Deng, Anan Li, ..., Hui Gong, Xiaoquan Yang, Xiangning Li

xqyang@hust.edu.cn (X.Y.)
lixiangning@mail.hust.edu.cn (X.L.)

HIGHLIGHTS
Modified LR-White resin embedding was proposed to embed large-volume tissues

Retarder α-methyl-styrene was added to prevent cracking during polymerization

Resin formula was modified to preserve multiple fluorescent proteins

Microstructure information was acquired from the brains of different species

Article

Scalable Resin Embedding Method for Large-Volume Brain Tissues with High Fluorescence Preservation Capacity

Ting Luo,[1,2,4] Lei Deng,[1,2,4] Anan Li,[1,2,3] Can Zhou,[1,2] Shuai Shao,[1,2] Qingtao Sun,[3] Hui Gong,[1,2,3] Xiaoquan Yang,[1,2,3,*] and Xiangning Li[1,2,3,5,*]

SUMMARY

Resin embedding is widely used to dissect the fine structure of bio-tissue with electron and optical microscopy. However, it is difficult to embed large-volume tissues with resin. Here, we modified the formula of LR-White resin to prevent the sample cracking during polymerization process and applied this method to the intact brains of mouse, ferret, and macaque. Meanwhile, we increased the fluorescence preservation rate for green fluorescent protein (GFP) from 73 ± 4.0% to 126 ± 3.0% and tdTomato from 60 ± 3.3% to 117 ± 2.8%. Combined with the whole-brain imaging system, we acquired the cytoarchitectonic information and the circuit information such as individual axon and boutons which were labeled with multiple fluorescent proteins. This method shows great potential in the study of continuous fine microstructure information in large-volume tissues from different species, which can facilitate the neuroscience research and help the understanding of the structure-function relationship in complex bio-tissues.

INTRODUCTION

With the development of neuroscience research, different lab animal models with specific advantages such as ferret (Long et al., 2020), marmoset (Lin et al., 2019), and macaque (Jennings et al., 2016) were widely used in different research fields. The non-human primate brain is more similar to the human brain in terms of structure, morphology, and pathology. Further research into the non-human primate brains has great potential for understanding the structure and function of the human brain and treating many neurological diseases, such as Alzheimer disease and Parkinson disease (Yang et al., 2014; Niu et al., 2015; Zhu et al., 2018). Acquisition of fine microstructures of different brain samples in three dimensions is essential for understanding the structure-function relationship of the nervous system and brain evolution across different species (Rochefort et al., 2012; Nishiyama et al., 2019). For example, the selective loss of thin spines in the primate brain predicts working memory impairment (Motley et al., 2018). Due to the large volume of brain samples, it is difficult to acquire the microstructures of the whole brain with conventional optical imaging approaches. Novel imaging techniques such as mechanic sectioning-based whole-brain imaging systems have been developed to acquire the fine microstructures of large-volume brain samples (Gong et al., 2016; Long et al., 2020).

Resin embedding of biological tissues is widely used for electron microscopy and light microscopy to obtain detailed microstructure information (Belu et al., 2016; Chen et al., 2008). Combining resin embedding methods and modern molecular labeling techniques with mechanic sectioning-based whole-brain imaging systems (Li et al., 2010; Gong et al., 2016), researchers have acquired continuous and complete neural structures with cytoarchitecture information simultaneously and reconstructed the morphology of the specific neurons at a sub-micron resolution (Gong et al., 2013; Yuan et al., 2015). However, current resin embedding techniques are only used for small samples such as the zebrafish embryo (Sullivan-Brown et al., 2011; Nixon et al., 2009), nematode (Schieber et al., 2017), and the whole mouse brain with the size of 0.4 cm^3, which is hard to be applied in large-volume brain samples that are over tens of cubic centimeters. According to previous studies, one of the major difficulties is that cracking may occur during polymerization of the resin, and the cracking degree increases with the increased volume and polymerization temperature of the resin block (Yondem et al., 2011). Also, the fluorescence, which is from the fluorescent proteins that are used for fine structure labeling, may be reduced significantly in the condition of long-term

[1]Britton Chance Center for Biomedical Photonics, Wuhan National Laboratory for Optoelectronics-Huazhong University of Science and Technology, #1037, Luoyu Road, Wuhan, Hubei 430074, China

[2]MoE Key Laboratory for Biomedical Photonics, School of Engineering Sciences, Huazhong University of Science and Technology, Wuhan, Hubei 430074, China

[3]HUST-Suzhou Institute for Brainsmatics, Suzhou 215125, China

[4]These authors contributed equally

[5]Lead Contact

*Correspondence: xqyang@hust.edu.cn (X.Y.), lixiangning@mail.hust.edu.cn (X.L.)

https://doi.org/10.1016/j.isci.2020.101717

dehydration, resin monomer infiltration, and high polymerization temperature (Yang et al., 2013; Ren et al., 2018). Therefore, preventing the brain sample from cracking while preserving its fluorescence intensity during resin embedding process is the key to solving large-volume bio-tissue embedding problems.

In the present study, we modified the resin formula to prevent cracking and preserve the fluorescence of multiple fluorescent proteins. With whole-brain imaging system, we acquired the cytoarchitectonic information and the fine structure information from the brains of different species at a single-cell resolution level. The boutons of axon terminals and dendritic spines labeled by GFP or tdTomato were distinguished in the continuous 3D data sets. Combined with the viral tracer technology, this method is extremely promising for obtaining neural connection information throughout the whole brain from different species, which in turn can help to understand the structure-function relationship of complex neural circuits and the evolution of brains among various species.

RESULTS

Prevention of Sample Cracking during Embedding the Large-Volume Tissues with Resin

Compared to other embedding methods, such as paraffin embedding and agarose embedding, resin embedding shows excellent sectioning properties and morphological preservation ability (Saber et al., 2015; Wittenburg et al., 2009). Among a wide range of resins, LR-White resin exhibits the low viscosity and fast permeation ability in biological tissues (Yang et al., 2013), which suggests its potential to be applied in large-volume tissues. However, cracking still occurred in samples when using LR-White resin for large-volume bio-tissue embedding, which makes the imaging unavailable. To overcome these disadvantages, we explored that the key influence factor exist in the polymerization process of LR-White. During the polymerization process, the methacrylic acid ester and bisphenol-A dimethacrylate were copolymerized by the radical initiator to form the rigid main chain, while bisphenol-A dimethacrylate was used as the cross-linking agent to form a network structure. The ester group of methacrylic acid ester and bisphenol-A dimethacrylate reacted with the residual amine group of the biological tissue in the presence of the radical initiator to generate amide groups and hydrogen bonds (Figure 1A). During the standard process, the free radical with high activity could initiate polymerization quickly and released a large amount of energy immediately, which could cause explosive polymerization and then cracking in the resin. Hence, reducing the polymerization speed may prevent the resin from cracking. We proposed to add a retarder named AMS (retarder α-methyl styrene) to slow down the polymerization rate during the resin polymerization process. AMS has conjugation effect and steric hindrance effect, which is helpful to slow down the polymerization speed (Jiang et al., 2008). In structure, the double bond of AMS can react with free radicals to reduce the reaction activity (Figure 1B). In this case, as the amount of released heat decreases, the cracking phenomenon in resin can be alleviated gradually.

The dose of retarder is critical to sample polymerization. Excessive amounts of retarder may deplete the free radical during the polymerization process and lead to incomplete polymerization, while insufficient retarder may not reduce the polymerization rate significantly and cannot prevent the sample from cracking. In order to choose the optimal dose of AMS, we tested cracking alleviating ability among AMS with gradient concentrations. The macaque brain blocks (each one was of the roughly 2 cm ✕ 2 cm ✕ 1 cm size; all blocks were taken from the prefrontal cortex of the macaque brain) were used for the polymerization test. The degree of cracking decreased with the increase of AMS concentration in the resin. When the concentration reached more than 4% during resin infiltration, incomplete polymerization occurred (Figure 1C). Interestingly, the resin still cracked or corrugated when there was less than 4% AMS. According to our tests, only with exact 4% concentration of AMS could the resin with the entire macaque block inside achieve homogeneous polymerization. These results indicated that 4% AMS yielded the most optimal polymerization effect (Figure 1C). By using this approach, we embedded the intact brains of different species, from mouse to macaque. The embedding process took 3 days–22 days depending on the size of the samples (Figures 1D and Tables 1 and 2). After embedding, the sample was placed on the fluorescence micro-optical sectioning tomography (fMOST) system for sectioning and imaging (Gong et al., 2016). The system consists mainly of a fixed diamond knife, a 3D translation stage, a mercury lamp as a light source, and a water bath. First, the entire specimen was immersed in the water bath containing propidium iodide (PI) solution for real-time staining. Sectioning was achieved via the relative movement between the fixed diamond knife and the 3D translation stage on which the sample was fixed. After sectioning, the smooth fresh surface was exposed and the sample was then taken full volumetric mosaic imaging. The mosaic imaging process is repeated until the entire sectioning surface was imaged (Figure 1D).
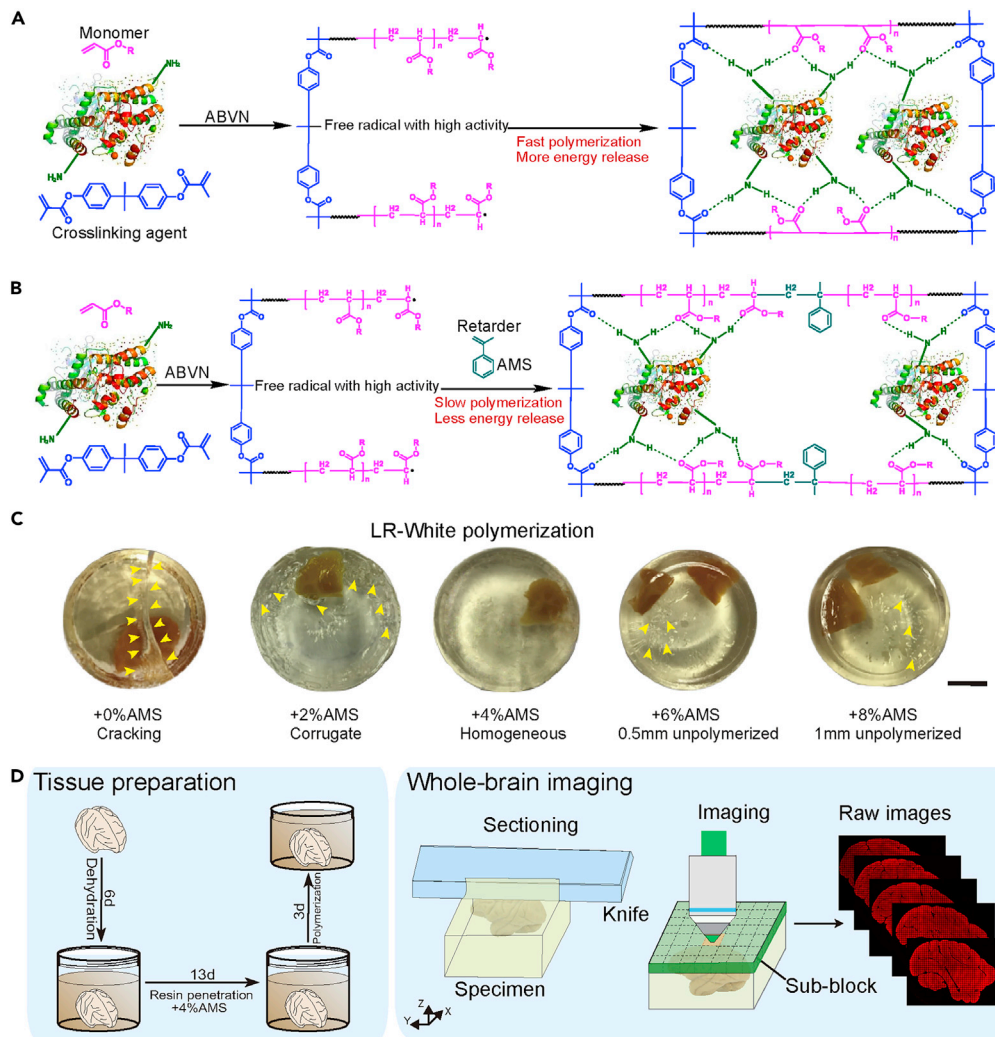
Figure 1. Modification of the Resin Embedding Method for Whole-Brain Imaging

(A) The reaction process of the resin polymerization including resin cross-linking with bio-tissue, the reaction between the ester group of the side chain and the residual amine group of the biological tissue. The monomer is methyl methacrylate and the cross-linking agent is bisphenol-A dimethacrylate, while the protein structure represents the embedded biological tissue.

(B) Reaction mechanism of retarder AMS to slow down the polymerization speed. The reaction between the double bond of AMS and free radical with high activity can generate free radical with low activity, which can reduce the rate of reaction and decrease the energy released in short time.

(C) The effect of different concentration of AMS retarder on LR-White polymerization. The arrows in 0% AMS indicate sample cracking after polymerization. Arrows in 2% AMS indicate corrugate on the surface of the resin after polymerization. Arrows in 6% AMS and 8% AMS indicate that the surface of the resin has not polymerized.

(D) Flowchart illustrating the procedure for embedding and imaging macaque brains. Scale bar in C, 2 cm.

The Improvement of Fluorescence Preservation Rate during the Resin Embedding Process

Although LR-White resin has been used to embed biological samples labeled with fluorescent protein (Brown et al., 2010; Keene et al., 2008), the fluorescence preservation rate is dissatisfactory. In previous studies, the fluorescence preservation rate of GFP and tdTomato after LR-White embedding was 76% and 27%, respectively (Yang et al., 2013; Xiong et al., 2014). To increase the fluorescence preservation rate of LR-White resin, we optimized the resin formula and embedding procedure. And to verify our method, we used ImageJ software to measure and quantify the fluorescence intensity before and after resin embedding. Briefly, the brain slices used for fluorescence quantification were first imaged before resin embedding. Then, the brain slices were embedded in LR-White and imaged again. The same neuron in

Tissues	Size/mm	Volume/cm^3	Dehydration	Resin Permeability	Polymerization
Mouse brains	21 × 11 × 11	0.4	9h	44h	38°C (24hr)
Rat brains	40 × 20 × 20	1.8	36h	132h	38°C (48hr)
Ferret brains	43 × 28 × 15	5.4	54h	168h	38°C (60hr)
Marmoset brains	30 × 25 × 18	8.0	72h	192h	38°C (60hr)
Macaque hemispheres	80 × 35 × 30	36	6d	13d	38°C (72hr)

Table 1. Resin Embedding Protocols for Tissues with Different Sizes
To optimize the resin embedding for different tissues, follow the protocol for the tissue with similar size and composition presented above and further optimize it if needed by changing dehydration and resin permeation time.

two images (before and after embedding) was identified, and the fluorescence was quantified with ImageJ. In one brain slice, usually 30–50 neurons were measured. All the brain slices were taken from three different animals.

In our previous studies, we have found that immersing resin-embedded brain samples labeled with GFP in alkaline solutions such as 0.05 M Na_2CO_3 solution could significantly increase the fluorescence intensity of GFP (Xiong et al., 2014). We referred this phenomenon as GFP reactivation. To verify the GFP reactivation with LR-White resin, we immersed the embedded GFP-labeled brain samples in 0.05 M Na_2CO_3 solution. The fluorescence intensity of GFP did increase remarkably (the fluorescence preservation rate improved from 42% to 73%, Figures 2A and 2B). However, as the same procedure applied to testing tdTomato preservation in brain slices (VIP-Cre mice crossed with Ai14 mice), no significant improvement of fluorescence intensity was found before and after alkaline solution immersion (preservation rate from 49% to 59%, Figure 2D), which was consistent with the previous study (Xiong et al., 2014). To increase the fluorescence intensity of tdTomato embedded in LR-White, further investigation needs to be performed. Firstly, we tried to remove the metal ions, which might quench the fluorescent signal of fluorescent proteins (Bae et al., 2018). We embedded the brain sections of the VIP-Cre:Ai14 mouse brain with LR-White resin and then immersed the embedded sections in 0.05 M Na_2CO_3 and ethylene diamine tetraacetic acid (EDTA) mixed solution with different EDTA concentrations. Only at a certain concentration range of EDTA, the fluorescence intensity of tdTomato increased significantly (from 59% to 109% by adding 0.05 M EDTA, Figures 2C and 2D), while in high or low concentration, the fluorescence intensity kept decreasing (Figure 2D). We identified that the most optimal concentration of EDTA solution is 0.05 M, which can also increase the fluorescence intensity of GFP (from 73% to 112%, Figure 2B).

It has also been reported that the lowering temperature was more favorable for the maintenance of fluorescence intensity of fluorescent proteins (Zhang et al., 2009). The required polymerization temperature can be lower when

Tissues	Dehydration (50%, 70%, 85%)	Dehydration (95%-1, 95%-2, 95%-3)	Permeability[a] (50%, 70%, 85%)	Permeability (100%-1, 100%-2, 100%-3)	Polymerization
Mouse brains	1h	2h	2h	12h/12hr/12hr	38°C (24hr)
Rat brains	6h	6h	12h	24h/24hr/48hr	38°C (48hr)
Ferret brains	8h	10h	24h	24h/24hr/48hr	38°C (60hr)
Marmoset brains	12h	12h	24h	36h/36hr/48hr	38°C (60hr)
Macaque hemispheres	24h	24h	48h	48h/48hr/72hr	38°C (72hr)

Table 2. Detailed Process Flow for Each Step of Different Samples
[a]50%, 70%, and 85% resin solution were a mix of 100% resin solution and 95% ethanol according to a certain weight ratio.

ABVN Concentration (%)	Temperature/ Polymerization Time (h)	24h	36h	48h	60h
0.10%	38°C	Unpolymerized	Unpolymerized	Unpolymerized	Unpolymerized
	40°C	Unpolymerized	Unpolymerized	Unpolymerized	Unpolymerized
	45°C	Polymerized	–	–	–
0.16%	38°C	Unpolymerized	Unpolymerized	Unpolymerized	Unpolymerized
	40°C	Unpolymerized	Polymerized	–	–
	45°C	Polymerized	–	–	–
0.24%	38°C	Polymerized	–	–	–
	40°C	Polymerized	–	–	–
	45°C	Polymerized	–	–	–

Table 3. Selection of Optimal Concentration of ABVN Initiator for LR-White Polymerization

the initiator is more active (Luo et al., 2002). Therefore, we replaced the low activity initiator benzoyl peroxide (Watanabe et al., 2010) with high activity initiator 2, 2-azobis-(2,4-dimethylvaleronitrile) (ABVN) (Liu et al., 2015). The concentration of ABVN also affected the polymerization temperature. We then tested the polymerization effect of the different amounts of ABVN in the resin at different temperatures. The best ABVN amount was 0.24 g in 100 g resin, and the corresponding polymerization temperature was 38°C (Table 3). To test the effect of lowering polymerization temperatures on GFP and tdTomato fluorescence retention, we selected adjacent 100-μm-thick brain sections of the Thy1-GFP mouse brain and VIP-Cre:Ai14 mouse brain and embedded the brain sections at 38°C and 60°C, respectively. The results showed that lowering embedding temperature can significantly improve the signal-to-noise ratio of the image (Figures 2E–2J).

Finally, we tested the comprehensive effects of adding EDTA solution and lowering the polymerization temperature on the fluorescence intensity of GFP and tdTomato. The 100-μm-thick brain slices of Thy1-GFP and VIP-Cre:Ai14 mouse brains were firstly embedded at 38°C, and then, we immersed the embedded brain slices in 0.05 M EDTA solution and 0.05 M Na_2CO_3 solution mixture to acquire the fluorescent images. The picture imaged in this process was transferred to ImageJ for florescence intensity measurement. The results showed that compared to the brain slices before embedding, the fluorescence preservation rate of GFP and tdTomato was $126 \pm 3.0\%$ and $117 \pm 2.8\%$, respectively, after modified LR-White embedding (Figures 2K–2M).

Acquisition of Cytoarchitectonic Information from the Brains of Different Species

To demonstrate that the modified method can be applied to different brain samples with various sizes, we embedded a macaque brain hemisphere (80 mm × 35mm × 30 mm) and an intact ferret brain (43 mm × 28 mm × 15 mm) (Figures 3A and 3C). Then, the embedded macaque brain hemisphere and intact ferret brain sample were imaged with fMOST at the lateral resolution of 0.64 μm × 0.64 μm and 0.32 μm × 0.32 μm, respectively. Both of the samples were continuously sectioned and imaged at intervals of 50 μm. Before each imaging-sectioning cycle, the exposed surface of the embedded sample was stained immediately by PI, which provided cytoarchitectonic information (Figure 3D). The PI staining was uniform and clear throughout the different planes, indicating that the resin effectively penetrated and could support the entire tissue block during the embedding process. Due to satisfactory resin embedding effects, the anatomical structure of the macaque brain and ferret brain can be clearly identified, and the white matter and the gray matter were easy to distinguish (Figures 3E and 3F). According to the cytoarchitecture, different brain areas such as the visual cortex, the dorsal side of the prefrontal cortex, and the part of the parietal lobe of the macaque brain can be clearly distinguished (Figure 3E).

We also identified the different brain regions in the ferret brain such as the striatum, thalamus, midbrain, and cerebellum (Figure 3F). We divided the regions of the macaque brain by distinguishing the cytoarchitecture, which is consistent with the Atlas of the Rhesus Monkey Brain (Paxinos et al., 1999) (Figure 3E). The
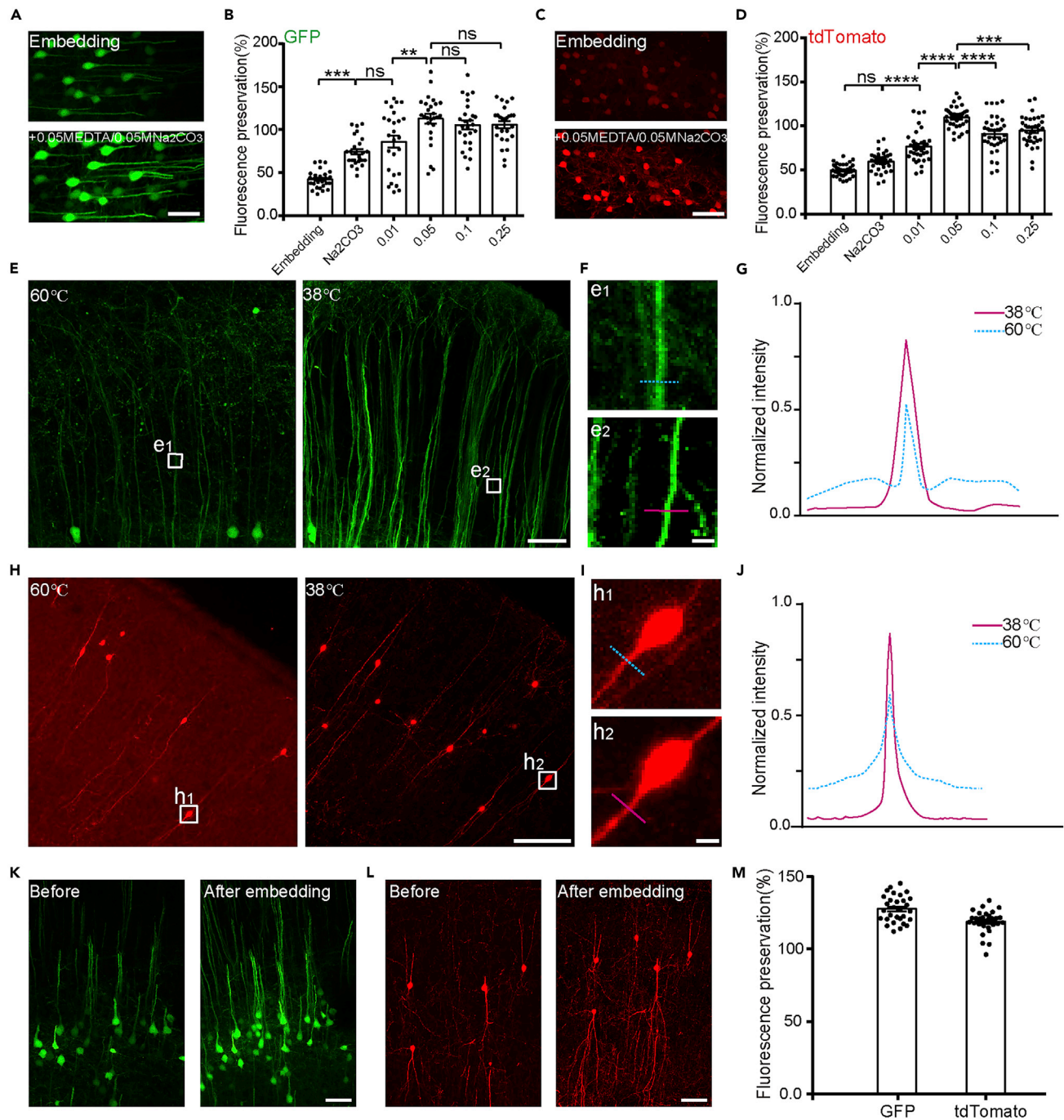
Figure 2. Improvement of Fluorescence Preservation Rate in LR-White Resin

(A)The GFP signals in LR-White embedded brain slices before and after alkaline solution (0.05 M Na$_2$CO$_3$ and 0.05 M EDTA mixture) activation.

(B) Quantitative results show the fluorescence preservation rate of GFP in different conditions (embedded in LR-White, embedded in LR-White and activated by 0.05 M Na$_2$CO$_3$, embedded in LR-White and activated by 0.05 M Na$_2$CO$_3$ and different concentration of EDTA mixture) (n = 26 cells for each group).

(C) The tdTomato signals in LR-White embedded brain slices before and after 0.05 M Na$_2$CO$_3$ and 0.05 M EDTA mixture activation.

(D) Quantitative results show fluorescence preservation rate of tdTomato in different conditions (embedded in LR-White, embedded in LR-White and activated by 0.05 M Na$_2$CO$_3$, embedded in LR-White and activated by 0.05 M Na$_2$CO$_3$ and different concentration of EDTA mixture) (n = 35 cells for each group).

(E) Details of GFP-labeled neurons in brain slices after embedding at 60°C and 38°C.

(F) An enlarged view of the area indicated in (E), showing the fibers around the soma after embedding at different temperatures.

(G) Fluorescence intensity plots for the lines labeled in (F).

Figure 2. *Continued*

(H) Details of tdTomato-labeled neurons in brain slices after embedding at 60°C and 38°C.

(I) An enlarged view of the area indicated in (H), showing the fibers around the soma after embedding at different temperatures.

(J) Fluorescence intensity plots for the lines labeled in (I).

(K and L) Fluorescence images of EGFP (Thy1-GFP-H mouse) and tdTomato (VIP-Cre:Ai14 mouse) in brain slices before and after modified LR-White resin embedding.

(M) GFP and tdTomato preservation rate after modified LR-White embedding (n = 30 cells for each group). Scale bars, (A, C, E) 50 μm; (H) 100 μm; (K, L) 50 μm; (F, I) 5 μm; Error bars represent standard error of mean (SEM). One-way analysis of variance (ANOVA) followed by Tukey's post hoc tests (*p < 0.05, **p < 0.01, ***p < 0.001, ****p < 0.0001, ns represents no significance).

different cortical layers and cell bodies in different cortical layers with different shape and size can be clearly identified in the high-resolution images (Figures 3G–3L). The different cerebellar layers of the macaque brain and ferret brain can also be visualized (Figures 3M–3O). These results demonstrated that the present method can be used to embed the brain samples with various sizes. Combining with our whole-brain imaging system, we can acquire the high-resolution cytoarchitectonic information from different brain samples of multiple species. These data sets can be used to build the three-dimensional high-resolution reference atlas of different animals.

The Preservation of Fluorescent Signals of Multiple Fluorescent Proteins during Large Sample Embedding

To prove the embedding method is suitable for the fluorescent protein in large-volume samples, we firstly embedded the intact brain of Thy1-GFP mouse. After embedding, we sectioned the whole brain with a sliding microtome (KD2508) to generate a smooth block face for imaging the corresponding sections. A mixture of 0.05 M EDTA solution and 0.05 M Na_2CO_3 solution was used to increase the fluorescent signals of GFP. We imaged the resin-embedded brain block at different coronal planes. The GFP signals were uniform and strong across different coronal planes of the embedded sample, while its intensity showed almost the same as the one across the sample which was placed directly in PBS solution and without embedding (Figure 4A). We also acquired the images of fine detailed neural structures in different brain regions such as the morphology of granule cells in the dentate gyrus of the hippocampus (Figures 4B–4D), the apical dendrites, and the dendritic spines of cortical pyramidal neurons (Figures 4E–4I), as well as the axon pathways in the pallidum (Figures 4J and 4K) and the projection neurons in the basolateral amygdala (Figures 4L and 4M). All these pictures showed clear details of microstructure, which indicated that the modified LR-White resin embedding method is suitable for large-volume samples labeled by GFP.

To validate the fluorescence preservation capability on tdTomato, we embedded the intact brain of SOM-Cre:Ai14 mouse. The somatostatin-positive (SOM+) neurons specifically express tdTomato. The embedded brain was processed to generate a smooth block face for imaging. A mixture of 0.05 M EDTA solution and 0.05 M Na_2CO_3 solution was also used to increase the fluorescent signals of tdTomato on the block face. We imaged the resin-embedded brain block and compared the fluorescent image with the image acquired from PFA-fixed brain slices in PBS solution (Figures 5A and 5B). The tdTomato fluorescent signals can be clearly visualized after modified LR-White embedding. We acquired the detailed images from the cortex, hippocampus, and amygdala. All the fine structures such as the apical dendrites of local SOM + neurons in the cortex (Figures 5C and 5D), axons and dendrites in the amygdala (Figures 5E–5G), as well as the axon terminals, dendrites, and dendritic spines in the hippocampus (Figures 5H–5K), were well preserved. These results demonstrated that the embedding method can be applied to tdTomato-labeled large-volume samples.

Detection of Viral Labeled Fluorescent Signals in the Macaque Brain

Given the high level of fluorescence preservation capability of our modified LR-White embedding method, it has the potential to detect microstructures with weak fluorescence signals. Here, we applied this method to visualize the neuronal connectivity of macaque brain tissues labeled with virus including adeno-associated virus (AAV)-GFP and AAV-tdTomato.

The macaque brain tissue blocks (2 × 2 × 1 cm³) labeled with AAV-GFP or AAV-tdTomato virus were embedded with LR-White resin. We found that the fine fluorescent signals and the neuronal morphological details were both well preserved after embedding. Combined with the whole-brain imaging system (Gong et al., 2016), the fluorescent protein-labeled soma signals and the continuous clusters of nerve fiber
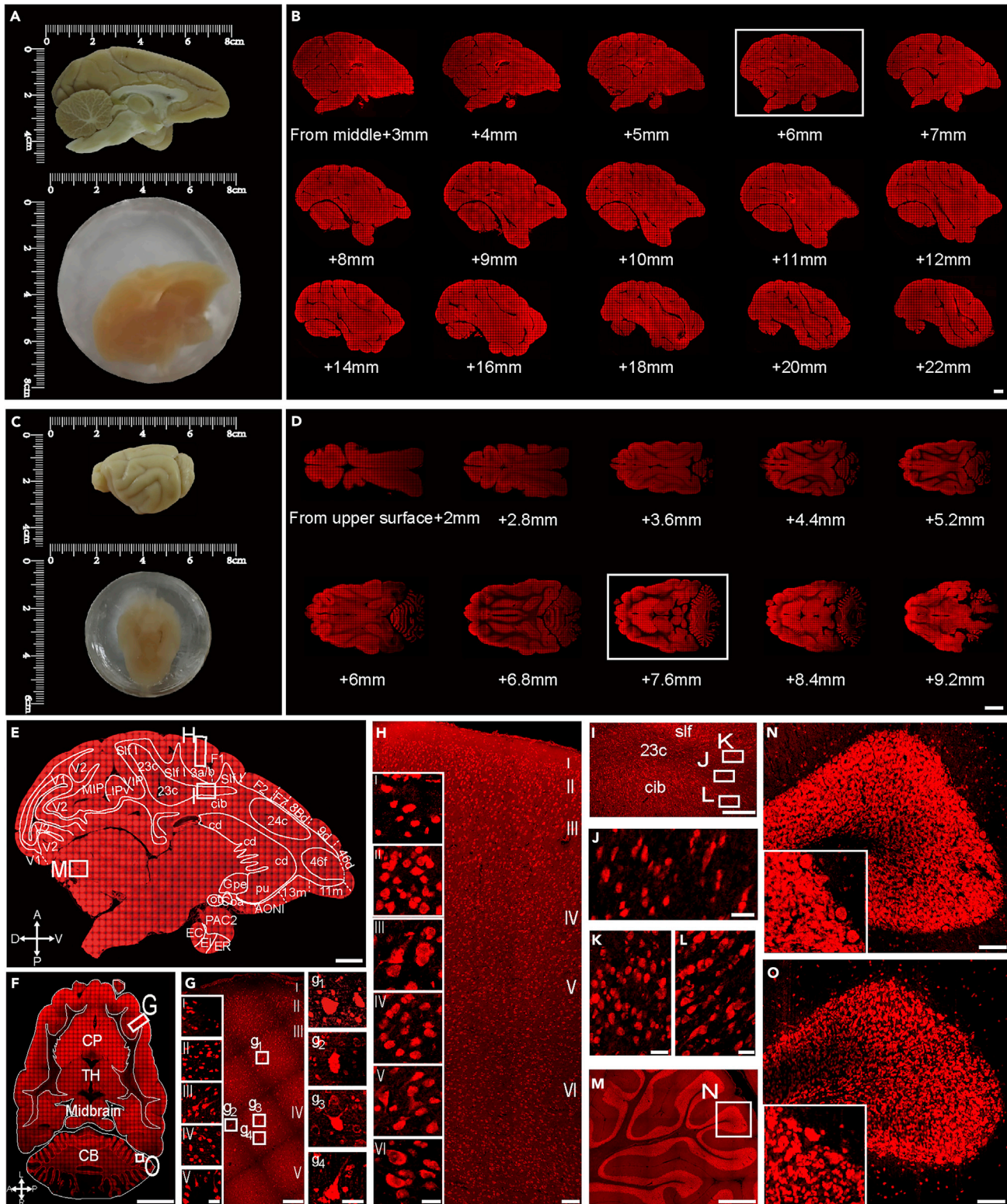
Figure 3. Acquisition of Cytoarchitectonic Information of the Macaque Brain and Ferret Brain with the Modified LR-White Embedding Method

(A) The picture of the PFA-fixed macaque brain (top) and the macaque brain after LR-White resin embedding (down).

(B) The macaque brain sagittal plane images of PI staining at intervals of 1–2 mm.

Figure 3. *Continued*

(C) The picture of the ferret brain before and after resin embedding.

(D) PI staining of horizontal plane interval from upper surface +2 mm to +9.2 mm.

(E) The images show the architectonic information of some brain region partitions of the macaque brain sagittal planes.

(F) PI staining results of horizontal planes of the ferret brain show different brain regions.

(G) The partial enlarged detail of (F) shows the different cell body morphology of different cortical layers in the ferret brain.

(H) The partial enlarged detail of (E) shows the different cell body morphology of different cortical layers in the macaque brain.

(I) An enlarged image of the rectangular area in figure (E).

(J–L) Enlarged views of the white boxes in (I) showing different cell body morphology.

(M) The enlarge views of the cerebellum from white blocks of (E).

(N) Images were obtained at corresponding magnification of the regions indicated in (M).

(O) An enlarge view of the cerebellar granulocytes indicated by the white square in (F). Superior longitudinal fasciculus, slf; cingulum bundle, cib; subregion of posterior cingulate cortex, 23c; caudate putamen, CP; thalamus, TH; cerebellum, CB; scale bars, (B, D, E, F) 1 mm; (G) 20 μm; 100 μm; 20 μm; (H) 20 μm; 100 μm; (I) 100 μm; (J-L) 20 μm; (M) 1 mm; (N-O) 100 μm.

bundles were obtained (Figures 6A–6E, and 6I–6J). Fine images of small and weakly labeled structures such as the tiny axons and buttons could be observed (Figures 6F–6H, and 6K). To demonstrate the high fluorescence preservation capacity of the modified LR-White embedding method, we also embedded the fluorescence-labeled macaque brain tissues with the standard LR-White embedding method. For the standard LR-White embedding method, we can see that the fluorescence signal is weak and the background is high after embedding, so the weak signal is submerged in the background and cannot be clearly visualized (Figures 6L–6N). Our results demonstrated that due to the high and stable fluorescence preservation capacity of optimized resin embedding, we can simultaneously achieve multi-color weak fluorescent signal detection of biological samples. Combined with multi-color fluorescent markers, three-dimensional imaging, and reconstruction, we can reconstruct the extensive and complex morphology of single neurons projecting throughout the entire primate brain, which can help understand the anatomical and functional organization of neural circuits in the non-human primate brain.

DISCUSSION

Investigations into the three-dimensional neural network of different brain structures from multiple species can contribute significantly to the overall understanding of the structure-function relationship and the brain evolution. To study the organization of the neural system with single-neuron resolution in three dimensions, the whole-brain three-dimensional imaging system has been developed (Gong et al., 2016). However, the resin embedding method suitable for various volume of brain tissues was lacked. Here, we modified the LR-White resin embedding method for multiple brain tissues, which was suitable for whole-brain high-resolution imaging and achieved excellent fluorescence preservation of various fluorescent proteins.

In present study, we choose LR-White resin as an embedding agent because of its good permeability and sectioning performance (Yang et al., 2013; Micheva et al., 2010). One of the most critical steps of embedding process is polymerization which can be triggered by UV, a catalyst, or heat. Due to the limited penetration depth of UV transmission in the biological tissue, it is not suitable for polymerization of large-volume samples (Erika et al., 2015). Catalytic polymerization is unstable and can be very easily inhibited by oxygen (Kim et al., 2020). Heat polymerization is more stable and easier to perform. Even so, when we applied LR-White resin to large-volume samples with heat polymerization, resin cracking occurred frequently. The resin cracking might be caused by a large amount of energy released in a short time during polymerization and shrinkage stress generated from the liquid to solid-state transmission of LR-White resin. We used AMS in resin polymerization process to weaken the activity of free radicals and slow down the polymerization rate of the resin (Sterling et al., 2001). We found that cracking could be alleviated and even eliminated at the certain ratio of added AMS into resin.

In the previous reports, LR-White has a poor fluorescence preservation capability (Yang et al., 2013) and especially for the red fluorescence that cannot be reactivated by alkaline solution after resin embedding (Xiong et al., 2014). This is probably because that the commonly used red fluorescent protein such as tdTomato was insensitive to pH (Xiong et al., 2014; Ren et al., 2018). In the present study, we found that high polymerization temperature may lead to the direct quenching of the weak signal during the embedding process. Lowering the temperature can protect the weak signal and improve the overall signal-to-background ratio. For tdTomato, the synergistic action of a metal ion chelating agent and carbonate ion was proposed to reactivate the quenched fluorescence. With these modifications, we ultimately achieved a
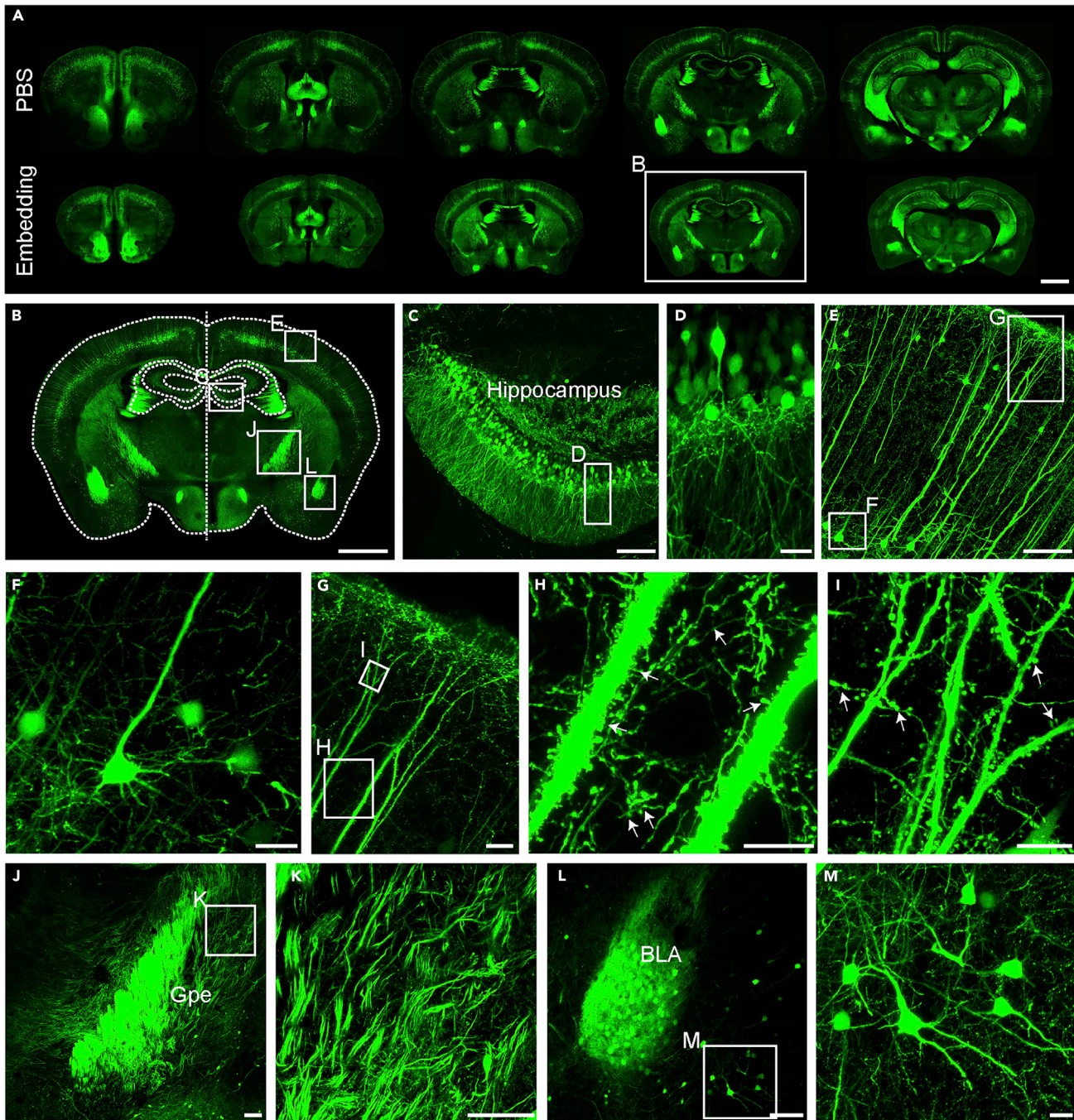
Figure 4. Embedding of Intact Brain of Thy1-GFP Mouse with the Modified LR-White Method Preserves the Fine GFP-Labeled Neuron Morphology

(A) Serial of different coronal planes show the uniform and strong GFP labeling in PBS and after embedding.

(B) A coronal plane shown in rectangle (A) that contains the cortex, hippocampus, amygdala, and pallidum after resin embedding.

(C) Enlarged hippocampal region in (B).

(D) The morphology of granule cells in the dentate gyrus of the hippocampus.

(E) GFP-labeled neurons in cortical regions.

(F) An enlarged view of the area indicated by the box in (E) shows the cell body of GFP-tlabeled neurons.

(G) An enlarged view of the area indicated by the box in (E) shows the apical dendrites.

(H and I) Enlarged image shows the dendritic spines and axon terminal in the white box of the image (G).

(J) Enlarged pallidum region in (B).

Figure 4. *Continued*

(K) An enlarged image in (J).

(L) Enlarged amygdala region in (B).

(M) An enlarged view of the area indicated by the white square in (L). Basolateral amygdaloid nucleus, BLA; globus pallidus, GPe; scale bars, (A-B) 1 mm; (C, E, J, K, L) 100 μm; (D, F, G, M) 20 μm; (H, I) 10 μm;

greater degree of improvement in the fluorescence preservation rate of GFP and tdTomato during the embedding process. It is noteworthy that resin embedding can cause sample shrinkage. Therefore, the increased brightness of fluorescent signals may be due to the increase in the concentration of fluorescent
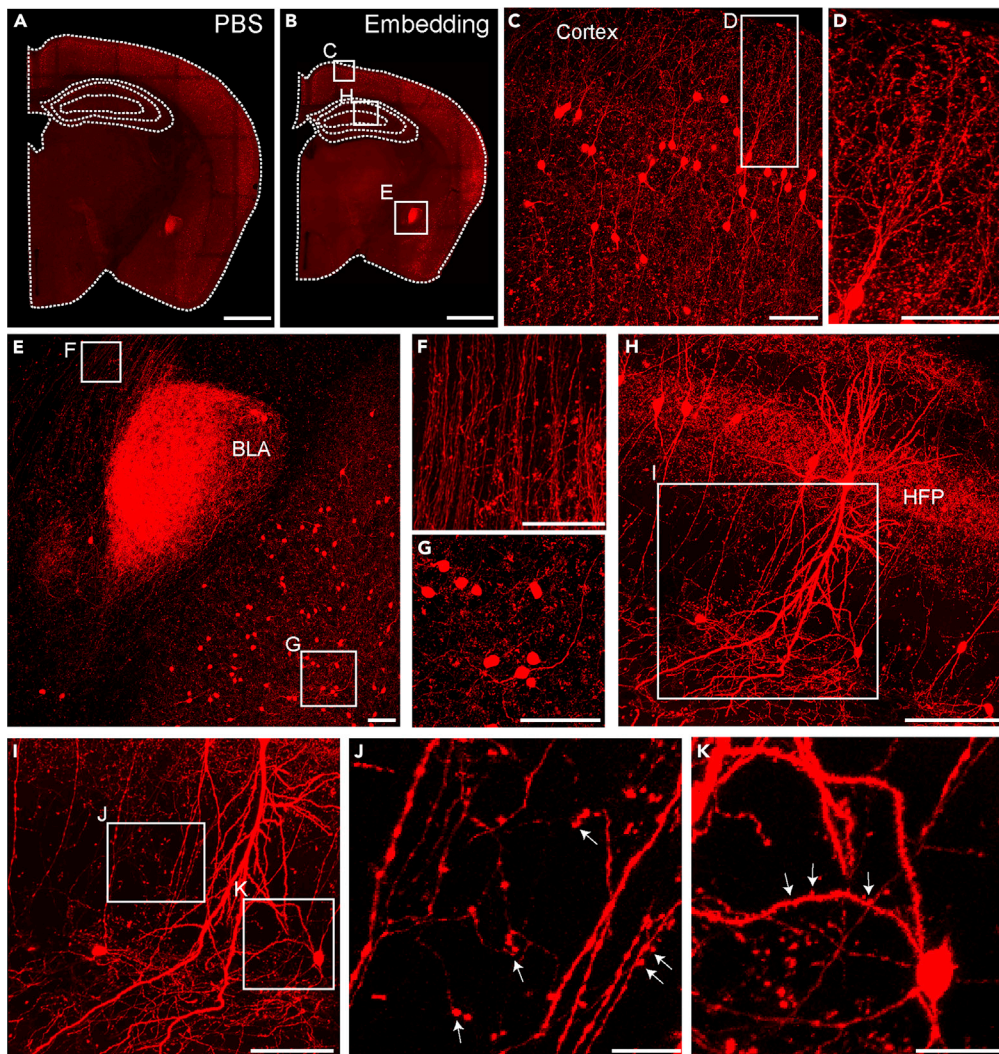
Figure 5. The Preservation of tdTomato Signals in the Mouse Brain After Embedding

(A and B) tdTomato fluorescent brain slices in PBS and after embedding.

(C) The enlarged image of the white box from (B) shows the morphology of somatostatin positive neurons in cortex.

(D) The partial enlarged detail of (C) shows the morphology of cortical dendrites.

(E) The enlarged image of the white box from (B).

(F and G) The partial enlarged detail of (E) shows the morphology of the fiber and soma in the amygdala after embedding.

(H) An enlarged image of the rectangular area in figure (B) shows the somatostatin-positive neurons in the hippocampus.

(I) The partial enlarged detail of (H) shows the details of the neurons in the hippocampus.

(J and K) An enlarged view of the area indicated by the rectangle in (I), demonstrating the visualization of axonal terminal and dendritic spines, which are indicated by white arrowheads. Scale bars, (A, B) 1 mm; (C-G) 50 μm; (H) 100 μm; (I) 50 μm; (J-K) 20 μm;
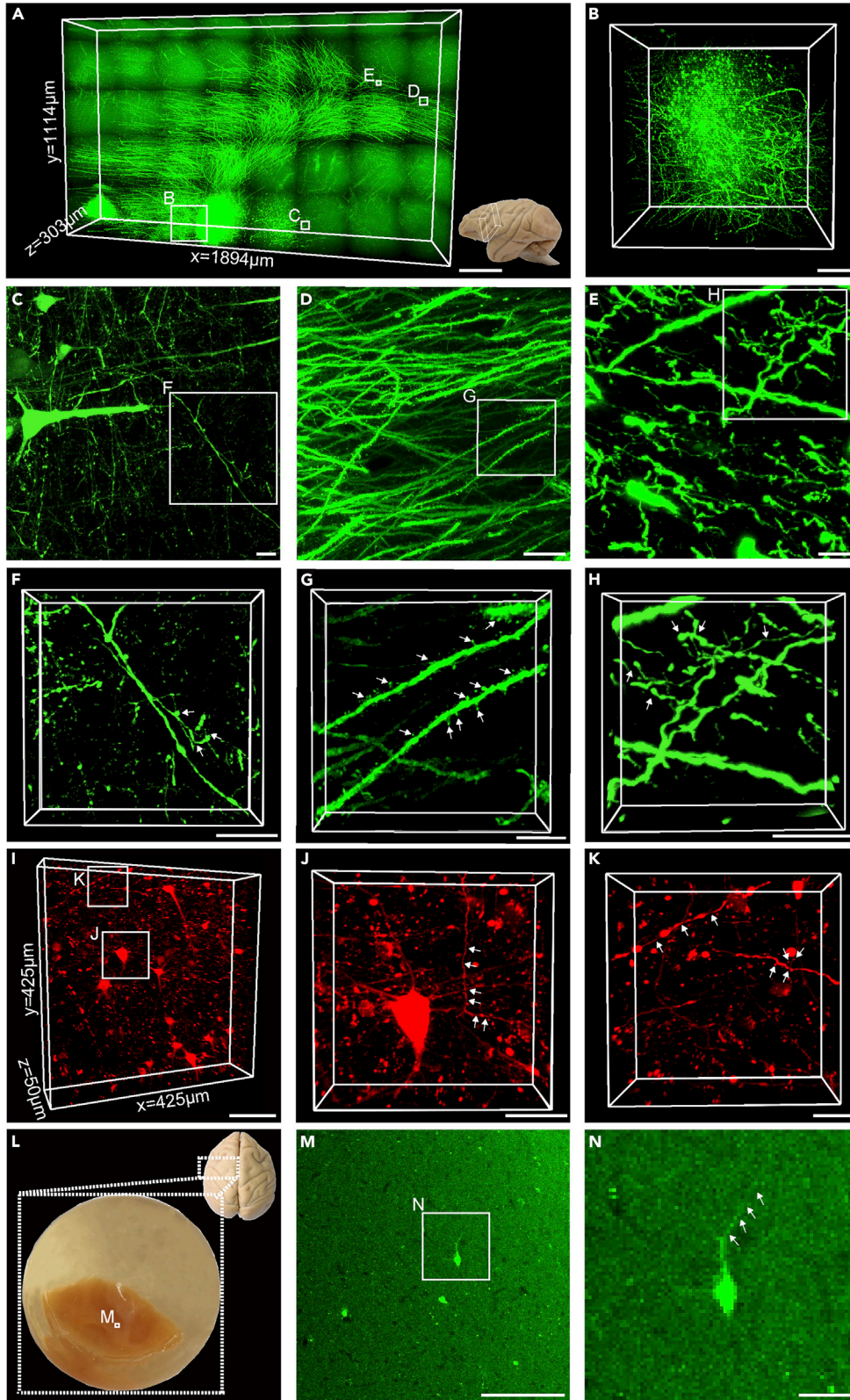
Figure 6. Acquisition of Neuronal Morphological Information in the Macaque Brain with Modified LR-White Embedding

(A) The regional signal of the injection site of the macaque brain blocks labeled with AAV-GFP after LR-White embedding.

(B)The enlarged image of the white box from (A), demonstrating the cell body and the fibers that emanate from the cell body in the injection site.

(C) Enlarged images of the selected regions of interest in (A).

(D and E) An enlarged view of the area indicated by the white rectangle in (A), demonstrating visualization of continuous of nerve fiber bundles.

(F) The image shows enlargements of the fine structures from the white box region of (C).

(G) Enlarged image in (D) shows the dendritic spine.

(H) Enlarged images in (E). White arrows indicate axon terminal and bouton.

(I) Local 3D signal presentation of an AAV-tdTomato-labeled macaque brain block after LR-White embedding.

(J and K) The image shows enlargements of the fine structures from the white box region of (I). White arrows indicate fine fiber and boutons.

(L) The picture of the macaque brain block before and after embedding.

(M) As shown in the white box in (L), demonstrated the macaque brain block signals after embedding.

(N) Enlargement of the white box in (M) shows the detailed signals after embedding. Scale bars, (A) 200 μm; (B) 50 μm; (C-E) 20 μm; (F) 30 μm; (G) 10 μm; (H) 30 μm; (I) 50 μm; (J) 30 μm; (K) 20 μm; (M) 50 μm; (N) 10 μm;

proteins caused by shrinkage. However, after standard LR-White embedding, the fluorescence intensity of both GFP and tdTomato decreased significantly (Figures 2A–2D), which indicated that the shrinkage caused by resin embedding alone cannot improve the fluorescence intensity of fluorescent proteins. Considering that both GFP and tdTomato have lots of homologous fluorescent proteins (Pakhomov and Martynov., 2008; Shaner et al., 2004), technically our method is also applicable to other fluorescent proteins that are homologous to GFP and tdTomato, such as BFP and mCherry.

Other embedding methods have also been developed to embed the large-volume brain tissues. For example, the paraffin embedding has been applied to embed the entire human brain and macaque brain hemisphere (Amunts et al., 2013; Zhanmu et al., 2020). Researchers also used dry ice to freeze the whole marmoset brain during the whole-brain imaging (Abe et al., 2017). Optical clearing methods can also be applied to large-volume tissues (Susaki et al., 2014). Compared to other embedding and tissue preparation methods, resin embedding has some unique advantages. First, resin-embedded biological tissues can be used to generate ultrathin sectioning. Therefore, the resin-embedded biological tissues can be collected and used for correlating light microscopy imaging and electron microscopy imaging (Micheva et al., 2010; Keene et al., 2008). Second, the biological tissues embedded in resin can be restored for a long time and are not easy to be affected by external environment during imaging and restoration. Therefore, the resin-embedded biological tissues can be used for long-term imaging.

Building three-dimensional brain reference atlas of different species has become a new research hotspot for neuroscience (Wang et al., 2020; Wu et al., 2014; Long et al., 2020). Whole-brain Nissl staining method has been developed for the building of three-dimensional brain reference atlas (Wu et al., 2014). However, the whole-brain Nissl staining usually takes weeks or even months to achieve uniform staining throughout the whole brain (Long et al., 2020), which is very time consuming. With our modified LR-White embedding, we can acquire the cytoarchitecture information of the whole brain with simultaneous PI staining during imaging (Figure 3) and skip the long-term Nissl staining procedure. Furthermore, the whole-brain Nissl staining can only be applied for bright field imaging, while our modified LR-White embedding method is capable of preservation of fluorescence of fluorescent proteins. Combined with our whole-brain imaging system, we can achieve acquisition of fluorescence-labeled neural structures and cytoarchitecture information simultaneously.

Overall, by overcoming the limitation of resin cracking and fluorescence quenching during resin embedding, we modified the LR-White resin embedding method to achieve high homogeneous polymerization and high level of fluorescence preservation for multiple brains from different species with various sizes. This method provides a new way for the study of large-volume brain tissues from mouse to non-human primate. In the future, with the throughput improvement of whole-brain imaging system, we hope that this method can be applied to acquiring the full morphology of a wider range of neurons in the intact brain of different species and contribute to the understanding of structure-function relationship in neural circuits and brain evolution research.

Limitations of the Study

In the present study, we have developed a resin embedding method suitable for large-volume samples such as ferret and macaque brains. Combined with the fMOST system, fine structural information was

obtained at a single-cell resolution. However, the amount of data acquired from high-resolution imaging system is enormous, which makes it difficult to restore, analyze, and share the relevant data sets. Recently, some progress has been made in big data storage and sharing. For example, a novel data compression method has been developed for big data storage (Economo et al., 2016). At the same time, algorithms for big data analysis and sharing such as the development of TDat (Li et al., 2017) and online tools for marmoset brain connectivity analysis (Majka et al., 2020) have been developed. With these new algorithms and tools, data sets of large mammalian brains can be accessed more freely.

Resource Availability

Lead Contact

Further information and requests for resources and reagents should be directed to and will be fulfilled by the lead contact, Xiangning Li (lixiangning@mail.hust.edu.cn).

Materials Availability

This study did not generate new unique reagents.

Data and Code Availability

We did not use any data sets.

METHODS

All methods can be found in the accompanying Transparent Methods supplemental file.

SUPPLEMENTAL INFORMATION

Supplemental Information can be found online at https://doi.org/10.1016/j.isci.2020.101717.

AUTHOR CONTRIBUTIONS

H.G. and X.L. conceived and designed the study. T.L. and C.Z. performed the experiments and data analysis. X.Y., L.D., A.L., and S.S. performed the whole-brain data acquisition. X.L., T.L., and Q.S. prepared the figures and wrote the manuscript.

DECLARATION OF INTERESTS

The authors declare that the research was conducted in the absence of any commercial or financial relationships that could be construed as a potential conflict of interest.

REFERENCES

Abe, H., Tani, T., Mashiko, H., Kitamura, N., Miyakawa, N., Mimura, K., Sakai, K., Suzuki, W., Kurotani, T., Mizukami, H., et al. (2017). 3D reconstruction of brain section images for creating axonal projection maps in marmosets. J. Neurosci. Methods *286*, 102–113.

Amunts, K., Lepage, C., Borgeat, L., Mohlberg, H., Dickscheid, T., Rousseau, M.E., Bludau, S.,

Bazin, P.L., Lewis, L.B., Oros-Peusquens, A.M., et al. (2013). BigBrain: an ultrahigh-resolution 3D human brain model. Science *340*, 1472–1475.

Bae, J.E., Kim, I.J., and Nam, K.H. (2018). Spectroscopic analysis of the Cu$^{(2+)}$-induced fluorescence quenching of fluorescent proteins amCyan and

mOrange2. Mol. Biotechnol. *60*, 485–491.

Belu, A., Schnitker, J., Bertazzo, S., Neumann, E., Mayer, D., Offenhausser, A., and Santoro, F. (2016). Ultra-thin resin embedding method for scanning electron microscopy of individual cells on high and low aspect ratio 3D nanostructures. J. Microsc. *263*, 78–86.

Brown, T.A., Fetter, R.D., Tkachuk, A.N., and Clayton, D.A. (2010). Approaches toward super-resolution fluorescence imaging of mitochondrial proteins using palm. Methods 51, 458–463.

Chen, X., Winters, C.A., and Reese, T.S. (2008). Life inside a thin section: tomography. J. Neurosci. 28, 9321.

Economo, M.N., Clack, N.G., Lavis, L.D., Gerfen, C.R., Svoboda, K., Myers, E.W., and Chandrashekar, J. (2016). A platform for brain-wide imaging and reconstruction of individual neurons. Elife 5, e10566.

Fantino, Erika, Vitale, A., Quaglio, M., Cocuzza, M., Pirri, C.F., and Bongiovanni, R. (2015). Blue and uv combined photolithographic polymerization for the patterning of thick structures. Chem. Eng. J. 267, 65–72.

Gong, H., Xu, D., Yuan, J., Li, X., Guo, C., Peng, J., Li, Y., Schwarz, L.A., Li, A., Hu, B., et al. (2016). High-throughput dual-colour precision imaging for brain-wide connectome with cytoarchitectonic landmarks at the cellular level. Nat. Commun. 7, 12142.

Gong, H., Zeng, S., Yan, C., Lv, X., Yang, Z., Xu, T., Feng, Z., Ding, W., Qi, X., Li, A., et al. (2013). Continuously tracing brain-wide long-distance axonal projections in mice at a one-micron voxel resolution. Neuroimage 74, 87–98.

Jennings, C.G., Landman, R., Zhou, Y., Sharma, J., Hyman, J., Movshon, J.A., Qiu, Z., Roberts, A.C., Roe, A.W., Wang, X., et al. (2016). Opportunities and challenges in modeling human brain disorders in transgenic primates. Nat. Neurosci. 19, 1123–1133.

Jiang, S., Deng, J., and Yang, W. (2008). Block copolymers prepared by free radical polymerization using α-Methylstyrene-containing precopolymer as macroinitiator. Polym. J. 40, 543.

Keene, D.R., Tufa, S.F., Lunstrum, G.P., Holden, P., and Horton, W.A. (2008). Confocal/TEM overlay microscopy: a simple method for correlating confocal and electron microscopy of cells expressing GFP/YFP fusion proteins. Microsc. Microanal. 14, 342–348.

Kim, S., and Sikes, H.D. (2020). Radical polymerization reactions for amplified biodetection signals. Polym. Chem. 11, 1424–1444.

Li, A., Gong, H., Zhang, B., Wang, Q., Yan, C., Wu, J., Liu, Q., Zeng, S., and Luo, Q. (2010). Micro-optical sectioning tomography to obtain a high-resolution atlas of the mouse brain. Science 330, 1404–1408.

Li, Y., Gong, H., Yang, X., Yuan, J., Jiang, T., Li, X., Sun, Q., Zhu, D., Wang, Z., Luo, Q., and Li, A. (2017). TDat: an efficient platform for processing petabyte-scale whole-brain volumetric images. Front. Neural circuits 11, 51.

Lin, M.K., Takahashi, Y.S., Huo, B.X., Hanada, M., Nagashima, J., Hata, J., Tolpygo, A.S., Ram, K., Lee, B.C., Miller, M.I., et al. (2019). A high-throughput neurohistological pipeline for brain-wide mesoscale connectivity mapping of the common marmoset. Elife 8, e40042.

Liu, Q., Liu, L., Ma, Y., Zhao, C., and Yang, W. (2015). A novel polymer chain growing mode and styrene copolymer prepared with low molecular weight copolymer of α-methylstyrene and styrene as macroinitiator. J. Appl. Polym. Sci. 132, 7.

Long, B., Jiang, T., Zhang, J., Chen, S., Jia, X., Xu, X., Luo, Q., Gong, H., Li, A., and Li, X. (2020). Mapping the architecture of ferret brains at single-cell resolution. Front. Neurosci. 14, 322.

Luo, Y., Yao, Y., and Shen, Q. (2002). [(SiMe₃)₂NC(NiPr)₂]₂Ln(μ-Me)₂Li(TMEDA) (Ln = Nd, Yb) as effective single-component initiators for styrene polymerization. Macromolecules 35, 8670–8671.

Majka, P., Bai, S., Bakola, S., Bednarek, S., Chan, J.M., Jermakow, N., Passarelli, L., Reser, D.H., Theodoni, P., Worthy, K.H., et al. (2020). Open access resource for cellular-resolution analyses of corticocortical connectivity in the marmoset monkey. Nat. Commun. 11, 1133.

Micheva, K.D., Busse, B., Weiler, N.C., O'Rourke, N., and Smith, S.J. (2010). Single-synapse analysis of a diverse synapse population: proteomic imaging methods and markers. Neuron 68, 639–653.

Motley, S.E., Grossman, Y.S., Janssen, W.G.M., Baxter, M.G., and Morrison, J.H. (2018). Selective loss of thin spines in area 7a of the primate intraparietal sulcus predicts age-related working memory impairment. J. Neurosci. 38, 10467–10478.

Nishiyama, J. (2019). Plasticity of dendritic spines: molecular function and dysfunction in neurodevelopmental disorders. Psychiatry Clin. Neurosci. 73, 541–550.

Niu, Y., Guo, X., Chen, Y., Wang, C.E., Gao, J., Yang, W., Kang, Y., Si, W., Wang, H., Yang, S.H., Li, S., Ji, W., Li, X.J., et al. (2015). Early Parkinson's disease symptoms in α-synuclein transgenic monkeys. Hum. Mol. Genet. 8, 2308–2317.

Nixon, S.J., Webb, R.I., Floetenmeyer, M., Schieber, N., Lo, H.P., and Parton, R.G. (2009). A single method for cryofixation and correlative light, electron microscopy and tomography of zebrafish embryos. Traffic 10, 131–136.

Pakhomov, A.A., and Martynov, V.I. (2008). GFP family: structural insights into spectral tuning. Chem. Biol. 15, 755–764.

Paxinos, G., Huang, X.-F., and Toga, A.W. (1999). The Rhesus Monkey Brain in Stereotaxic Coordinates (Academic Press).

Ren, M., Tian, J., Zhao, P., Luo, J., Feng, Z., Gong, H., and Li, X. (2018). Simultaneous acquisition of multicolor information from neural circuits in resin-embedded samples. Front. Neurosci. 12, 885.

Rochefort, N.L., and Konnerth, A. (2012). Dendritic spines: from structure to in vivo function. EMBO Rep. 13, 699–708.

Saber, Sámar, Macías, David, Josetxu, O.D.U., and Kjesbu, O.S. (2015). Stereological comparison of oocyte recruitment and batch

fecundity estimates from paraffin and resin sections using spawning albacore (thunnus alalunga) ovaries as a case study. J. Sea Res. 95 (jan), 226–238.

Schieber, N.L., Machado, P., Markert, S.M., Stigloher, C., Schwab, Y., and Steyer, A.M. (2017). Minimal resin embedding of multicellular specimens for targeted FIB-SEM imaging. Methods Cell Biol. 140, 69–83.

Shaner, N.C., Campbell, R.E., Steinbach, P.A., Giepmans, B.N., Palmer, A.E., and Tsien, R.Y. (2004). Improved monomeric red, orange and yellow fluorescent proteins derived from Discosoma sp. red fluorescent protein. Nat. Biotechnol. 22, 1567–1572.

Sterling, W.J., Kim, Y.-C., and McCoy, B.J. (2001). Peroxide enhancement of poly(α-methylstyrene) thermal degradation. Ind. Eng. Chem. Res. 40, 1811–1821.

Sullivan-Brown, J., Bisher, M.E., and Burdine, R.D. (2011). Embedding, serial sectioning and staining of zebrafish embryos using jb-4 resin. Nat. Protoc. 6, 46–55.

Susaki, E.A., Tainaka, K., Perrin, D., Kishino, F., Tawara, T., Watanabe, T.M., Yokoyama, C., Onoe, H., Eguchi, M., Yamaguchi, S., et al. (2014). Whole-brain imaging with single-cell resolution using chemical cocktails and computational analysis. Cell 157, 726–739.

Wang, Q., Ding, S.L., Li, Y., Royall, J., Feng, D., Lesnar, P., Graddis, N., Naeemi, M., Facer, B., Ho, A., et al. (2020). The allen mouse brain common coordinate framework: a 3D reference atlas. Cell 181, 936–953 e20.

Watanabe, S., Punge, A., Hollopeter, G., Willig, K.I., Hobson, R.J., Davis, M.W., Hell, S.W., and Jorgensen, E.M. (2010). Protein localization in electron micrographs using fluorescence nanoscopy. Nat. Methods 8, 80.

Wittenburg, G., Volkel, C., Mai, R., and Lauer, G. (2009). Immunohistochemical comparison of differentiation markers on paraffin and plastic embedded human bone samples. J. Physiol. Pharmacol. 60 (Suppl 8), 43–49.

Wu, J., He, Y., Yang, Z., Guo, C., Luo, Q., Zhou, W., Chen, S., Li, A., Xiong, B., Jiang, T., and Gong, H. (2014). 3D BrainCV: simultaneous visualization and analysis of cells and capillaries in a whole mouse brain with one-micron voxel resolution. Neuroimage 87, 199–208.

Xiong, H., Zhou, Z., Zhu, M., Lv, X., Li, A., Li, S., Li, L., Yang, T., Wang, S., Yang, Z., et al. (2014). Chemical reactivation of quenched fluorescent protein molecules enables resin-embedded fluorescence microimaging. Nat. Commun. 5, 3992.

Yang, M., Miao, J., Rizak, J., Zhai, R., Wang, Z., Huma, T., Li, T., Zheng, N., Wu, S., Zheng, Y., et al. (2014). Alzheimer's disease and methanol toxicity (part 2): lessons from four rhesus macaques (macaca mulatta) chronically fed methanol. J. Alzhmers Dis. 41, 4.

Yang, Z., Hu, B., Zhang, Y., Luo, Q., and Gong, H. (2013). Development of a plastic embedding method for large-volume and fluorescent-protein-expressing tissues. PLoS One *8*, e60877.

Yondem, I., Altintas, S.H., and Usumez, A. (2011). Temperature rise during resin composite polymerization under different ceramic restorations. Eur. J. Dentistry *5*, 305–309.

Yuan, J., Gong, H., Li, A., Li, X., Chen, S., Zeng, S., and Luo, Q. (2015). Visible rodent brain-wide networks at single-neuron resolution. Front. Neuroanat. *9*, 70.

Zhang, C., Liu, M.-S., and Xing, X.-H. (2009). Temperature influence on fluorescence intensity and enzyme activity of the fusion protein of GFP and hyperthermophilic xylanase. Appl. Microbiol. Biotechnol. *84*, 511–517.

Zhanmu, O., Yang, X., Gong, H., and Li, X. (2020). Paraffin-embedding for large volume bio-tissue. Sci. Rep. *10*, 12639.

Zhu, Y., Sousa, A.M.M., Gao, T., Skarica, M., Li, M., Santpere, G., Esteller-Cucala, P., Juan, D., Ferrández-Peral, L., Gulden, F.O., et al. (2018). Spatiotemporal transcriptomic divergence across human and macaque brain development. Science *362*, eaat8077.

Supplemental Information

Scalable Resin Embedding Method

for Large-Volume Brain Tissues with High

Fluorescence Preservation Capacity

Ting Luo, Lei Deng, Anan Li, Can Zhou, Shuai Shao, Qingtao Sun, Hui Gong, Xiaoquan Yang, and Xiangning Li

Materials and methods

Animals

Eight-week-old *thy1-GFP M-line* transgenic mice (Jackson Laboratory, Bar Harbor, ME, USA), *Som-Cre::Ai14* and *Vasoactive intestinal peptide-positive (VIP)-Cre::Ai14* transgenic mice (Huang Lab, Cold Spring Harbor Laboratory, Cold Spring Harbor, NY, USA), ferret (Wang Xiaoqun lab, Institute of Biophysics, Chinese Academy of Sciences) and macaque (Kunming institute of zoology, Chinese Academy of Sciences) were used in this study. Mice were kept in a 12-hour light/dark cycle with food and water available at will. All the procedures of animal experiments approved by the Institutional Animal Ethics Committee of the Huazhong university of Science and technology. All experiments were conducted in accordance with relevant governmental and institutional guidelines for the use of experimental animals.

Tissue preparation

Mice were deeply anesthetized with 1% solution of sodium pentobarbital (1% wt/vol) and subsequently perfused with 0.01 M phosphate buffered saline (PBS, Sigma-Aldrich Inc., St Louis, MO, USA)to flush the blood vessels, then followed by perfusion with 4% (1%wt/vol) paraformaldehyde(PFA, Sigma-Aldrich Inc., St Louis, MO, USA) and 2.5% sucrose in 0.01 M PBS for fixation. The brains were excised and post-fixed in 4% paraformaldehyde at 4 °C for 24 h. After fixation, the intact brain was rinsed overnight at 4 °C in a 0.01 M PBS solution. For tissue sections, we acquire 0.1-1 mm thick brain slices using a vibration microtome (Leica, VT1000 S).

The method of resin embedding

For 100-μm mouse brain slices, which were dehydrated in a graded ethanol series (50, 70, 85 and 95% ethanol, changing from one concentration to the next every 5 min at 4 °C). After dehydration, the brain slices were immersed in a graded LR-White series (Ted Pella Inc., Redding, CA, USA) (50, 70, 85, 100% LR-White for 15min each and 100% LR-White overnight at 4 °C). For mouse whole brain embedding, each intact brain was dehydrated in a graded ethanol series (50, 70 and 85% ethanol, changing from one concentration to the next every 1 h at 4 °C, and 95%

ethanol incubate the samples for 2 h each time, change the ethanol solution three times) and immersed in a graded LR-White series (50, 70, 85 and 100% resin)for 2 h each and 100% LR-White overnight for 36 h at 4 °C (change the solution once at 12 h). Subsequently, the samples were embedded in a vacuum oven at 38 °C for 24 h. The 100% LR-White solution comprised 100 g LR-white and 0.24 g ABVN as an initiator. The 70% and 85% LR-White solutions (wt/wt) were prepared from 95% ethanol and 100% LR-White.

For ferret brains, A graded series of ethanol solutions were used to dehydrate the tissue (four solutions were used: 50, 75, and 85%, each incubated for 8 h at 4 °C, and 95% ethanol incubated for 10 h each, change the solution three times). After dehydration, the samples were immersed in a graded series of LR-White (Ted Pella Inc., Redding, CA, USA) infiltration solutions, including 4% -AMS (Sigma-Aldrich M80903)(50, 70, 85% LR-White for 24 h each and 100%-1 LR-White for 24 h, 100%-2 LR-White for 24 h and 100%-3 LR-White for 48 h at 4 °C). Then the samples were embedded in a vacuum oven at 38 °C for 60 h.

Embedding procedures were performed on the macaque hemispheres, a graded series of ethanol solutions was used to dehydrate the tissue (four solutions were used: 50, 70, 85, 95, 95 and a third 95% (w/w), each incubated with the tissue for 24 h at 4 °C). The brain exhibited shrinkage slightly after dehydration, then the sample was ready for infiltration, it was successively immersed in a graded series of LR-White (Ted Pella Inc., Redding, CA, USA) infiltration solutions, including 4% -AMS (Sigma-Aldrich M80903)(50, 70, 85 and 100% LR-White for 48 h each and 100% LR-White 5 d at 4 °C, changed every 2 d). Then the sample was transferred to a sample bottle with a diameter of 8 cm and immersed in LR-White polymerization solution. The sample bottle was cured in a vacuum oven at 38 °C for 3 d. The virus-labeled macaque brain blocks were implanted in the way of the macaque hemispheres.

The macaque brain and ferret brain imaging

To obtain the cell construction information of the ferret and macaque brain, the sample was placed on the fMOST system to sectioning and imaging (Gong et al.,

2016). The whole sample was immersed in a water bath that containing PI solution for real-time staining. Whole-brain imaging was performed in the water bath. Sectioning was achieved through a relative motion between the fixed diamond knife and the 3D translation stage, after a smooth fresh surface was exposed, the sample was imaged subsequently, the full-volumetric imaging was performed with the cycle of sectioning and mosaic imaging, and the mosaic imaging process was repeated until the entire coronal section was acquired. In our experiment, the ferret macaque brain was imaged with a lateral resolution of 0.32×0.32 μm and 0.64×0.64 μm, respectively. For viral labeled macaque brain block imaging, the LR-white resin embedded macaque brain block was also imaged with fMOST system with two channels (GFP and tdTomato).

Confocal imaging

To evaluate fluorescence retention after embedding, we used 100 μm *thy1-GFP* and 100 μm *VIP-Cre: Ai14* mouse brain slices. The slices were first imaged with a commercial confocal microscope (Zeiss, LSM710) at 25 °C in 0.01 M PBS (Sigma-Aldrich Inc., St Louis, MO, USA). Imaging begins with tissue surface and terminate until no fluorescence signal, with a total imaging depth of approximately 30 μm, and scan at 2 μm intervals. Then we embed the imaged brain slices with LR-White resin and infiltrated the brain slices with 0.05 M/EDTA$+0.05$ M/Na_2CO_3 buffer or EDTA$+0.05$ M/Na_2CO_3 mixture solution with different concentration of EDTA, and then the microscope was set to the same configuration as the brain slices were first imaged.

To demonstrate fluorescence signal of the Thy1-GFP and SOM-Cre: Ai14 mouse brain after resin embedding, the commercial confocal microscope (Leica TCS SP8) was used to image. Imaging begins with tissue surface and terminates until the fluorescence signals can't be captured, with a total imaging depth of about 20 μm, and the microscope is scanned at 1 μm intervals. Before imaging, the sample were penetrated by 0.05 M/EDTA$+0.05$ M/Na_2CO_3 buffer for 2 min.

Fluorescence Preservation Quantitative Analysis

We used the ImageJ software to analyze the fluorescence preservation rate of the neurons. Specific steps: first, find the same neuron in the first-round imaging (before

embedding, i.e. the control group) and second round imaging (after embedding, i.e. the experimental group) of the raw data. Using elliptical or brush selection tools to select a region of interest in the soma of the neuron. Second, using ImageJ →Analyze→ Histogram tool to obtain the mean fluorescence of the selected region. It is assumed that the mean fluorescence of the control group was "A", the mean fluorescence of the experimental group was "B", and the sample fluorescence retention rate was "C", Then C was calculated according to the following formula: C=B/A*100%. In order to reduce the error, we usually measured 30-50 neurons in one image, then calculated the average values. We calculated at least three datasets (obtained from three different animals) for each group. For figures 2B, 2D and 2M, we used the above method to calculate the residual fluorescence preservation rate. Each point in fig2B, 2D and 2M represented the average fluorescence retention rate obtained from one brain slice (For each brain slice, 30-50 neurons were measured with ImageJ). All the brain slices were obtained from three different animals.

Statistics

All statistical graphs were generated using GraphPad Prism 7.01. The two-tailed student's t-test and one-way ANOVA followed by Tukey's post hoc tests were also performed using Graphpad Prism 7.01. The confidence level was set to 0.05 (P value), and all results were presented as the means ± SEM.